Available online at www.sciencedirect.com
SCIENCE DIRECT
Journal of Magnetic Resonance 181 (2006) 9–20
JMR Journal of Magnetic Resonance
www.elsevier.com/locate/jmr

A large volume flat coil probe for oriented membrane proteins

Peter L. Gor'kov [a,*], Eduard Y. Chekmenev [a], Riqiang Fu [a], Jun Hu [a], Timothy A. Cross [a,b], Myriam Cotten [c], William W. Brey [a]

[a] National High Magnetic Field Laboratory, Tallahassee, FL 32310, USA
[b] Department of Chemistry and Biochemistry, Florida State University, Tallahassee, FL 32306, USA
[c] Department of Chemistry, Pacific Lutheran University, Tacoma, WA 98447, USA

Received 20 December 2005; revised 1 March 2006
Available online 3 April 2006

Abstract

^{15}N detection of mechanically aligned membrane proteins benefits from large sample volumes that compensate for the low sensitivity of the observe nuclei, dilute sample preparation, and for the poor filling factor arising from the presence of alignment plates. Use of larger multi-tuned solenoids, however, is limited by wavelength effects that lead to inhomogeneous RF fields across the sample, complicating cross-polarization experiments. We describe a 600 MHz ^{15}N–^{1}H solid-state NMR probe with large (580 mm^3) RF solenoid for high-power, multi-pulse sequence experiments, such as polarization inversion spin exchange at the magic angle (PISEMA). In order to provide efficient detection for ^{15}N, a 4-turn solenoidal sample coil is used that exceeds 0.27λ at the 600 MHz ^{1}H resonance. A balanced tuning-matching circuit is employed to preserve RF homogeneity across the sample for adequate magnetization transfer from ^{1}H to ^{15}N. We describe a procedure for optimization of the shorted $1/4\lambda$ coaxial trap that allows for the sufficiently strong RF fields in both ^{1}H and ^{15}N channels to be achieved within the power limits of 300 W ^{1}H and 1 kW ^{15}N amplifiers. The $8 \times 6 \times 12$ mm solenoid sustains simultaneous B_1 irradiation of 100 kHz at ^{1}H frequency and 51 kHz at ^{15}N frequency for at least 5 ms with 265 and 700 W of input power in the respective channels. The probe functionality is demonstrated by 2D ^{15}N–^{1}H PISEMA spectroscopy for two applications at 600 MHz.

Keywords: PISEMA; Solid state NMR; Balanced circuit; Membrane protein; Coaxial trap; Flat coil

1. Introduction

Solid-state NMR methods that derive structural and orientational restraints from aligned samples have become valuable tools for studying difficult to approach, but biologically important membrane proteins [1–4]. Polarization inversion spin exchange at the magic angle (PISEMA) [5,6] has been widely used to obtain orientational restraints from membrane proteins in a lipid environment [7,8]. In dealing with oriented membrane protein samples, the proteins are inherently dilute due to the presence of lipids and multiple glass plates that macroscopically align the hydrated lipid bilayers containing protein or peptide. The use of a hermetically sealed container further decreases the filling factor and the already low sensitivity of ^{15}N detection often results in signal-to-noise inadequate for most multidimensional NMR experiments. Therefore, when protein production is not an issue, use of at least 100 μL of sample material is preferred for a successful experiment. When accounting for alignment plates and a sealed container, ~500 μL coil volumes are required for sufficient sensitivity.

Apart from an efficient ^{15}N detection channel in the RF probe, PISEMA experiments place strong demands on the decoupling channel, making larger sample coils hard to implement at high fields. While dipolar interactions are independent of the field strength, isotropic and anisotropic chemical shift interactions increase linearly with field. An intense B_1 field must be delivered to the sample to fully excite or decouple all spins of interest. This problem is amplified for multiple pulse sequences designed to

* Corresponding author. Fax: +1 850 644 1366.
E-mail address: pgorkov@magnet.fsu.edu (P.L. Gor'kov).

1090-7807/$ - see front matter © 2006 Elsevier Inc. All rights reserved.
doi:10.1016/j.jmr.2006.03.008

characterize dipolar couplings and anisotropic chemical shifts at high resolution requiring high power ^{1}H and ^{15}N RF pulses with multi-millisecond durations. However, because protein samples have significant RF loss at ^{1}H frequency, the large B_1 can easily damage the sample. For the present application, we believe that achieving a ^{1}H B_1 field of 100 kHz for non-lossy or 50 kHz for lossy samples, together with ^{15}N B_1 field of 50 kHz is an appropriate requirement. Desired RF field values should be achievable in the large coil within the power limits imposed by the available RF amplifiers, in our case—300 W for ^{1}H and 1 kW for ^{15}N frequency—a modest arrangement available in most solid state NMR labs. Good RF field homogeneity at both frequencies for cross-polarization (CP) across the sample is another pre-requisite that is harder to achieve in large coils.

Variations of the Cross–Hester–Waugh (CHW) RF circuit [9] are often used for CP probes [10–12]. One side of a sample solenoid is matched to the observe channel, and the other side is matched to the ^{1}H decoupling channel. A resonant trap is used to create a ^{1}H ground on the observe side of the coil, and a second trap provides an observe ground on the ^{1}H side. The coil is designed with a sufficient number of turns to provide good observe sensitivity at the expense of ^{1}H efficiency. An advantage of this approach is that having a single coil for both channels would seem to ensure a close match between the observe and ^{1}H RF fields. However, as coil size and frequency increase, extra care is required to obtain satisfactory performance with the CHW approach. Paulson and colleagues [13] have shown that a significant ^{1}H inhomogeneity starts to occur when the electrical length of the solenoid exceeds 10% of the ^{1}H wavelength. Such inhomogeneity becomes severe as the coil approaches 1/4 of the ^{1}H wavelength and further undermines the cross-polarization condition. An aqueous sample, in which the speed of light is slowed to approximately 1/8th of its free space value, also affects the electrical length of the coil. Additionally, physically large capacitors are needed to handle the currents and voltages that are required to produce adequate B_1 in a larger solenoid. At high frequency, the self-resonance of these capacitors interferes with the matching network and cannot be ignored.

Here, we present a design for a large sample volume, double resonance, ^{1}H–^{15}N solid-state NMR probe that overcomes the above mentioned difficulties and has been used to carry out successful 2D PISEMA experiments at 600 MHz. We describe and discuss the operation of the RF circuit, including a circuit modification that allows a coil that is $>1/4\lambda$ to produce a uniform RF field that nearly matches the ^{15}N field. The RF losses due to traps in the RF circuitry are analyzed. Custom-made traps to balance the efficiencies of the two channels for use in PISEMA experiments are described. Finally, the probe functionality is demonstrated by 2D ^{1}H–^{15}N PISEMA spectroscopy. Two important membrane protein systems are used here to demonstrate the capabilities of the probe design. The first is from the M2 protein exposed in the influenza A viral coat where it forms a proton channel. This protein has a simple transmembrane helix and as a tetramer it forms the biologically functional state. Even the transmembrane domain (M2-TMD) alone forms a functional tetrameric state and the backbone structure of this construct has been characterized by solid-state NMR [7,14–16]. In this symmetric bundle of helices the helical tilt to the bilayer normal is $37 \pm 3°$ [17]. Amantadine is an approved drug that binds to M2 protein, blocks the channel and the viral lifecycle. Here, PISEMA spectra of M2-TMD with bound amantadine are presented. Spectra are also obtained from the antimicrobial peptide, piscidin-1, from mast cells of fish [18]. Piscidin-1 is an amphipatic helix that in our preparation interacts with the lipid bilayer interfacial region [Chekmenev et al., unpublished results]. Piscidin-1 does not have a reported structure and the sample preparation employed here is one of the first steps towards structural and functional characterization of this antimicrobial peptide.

2. Methods

2.1. General

Due to the rectangular nature of uniformly aligned samples prepared with glass slides, a close-fitting rectangular solenoid is employed to achieve the best filling factor for detecting weak ^{15}N signals from membrane proteins. The exact inner dimensions of the sample solenoid have evolved around the glass plates and rectangular glass cells used for sample preparation in our laboratory, as described in more detail below. The large, 4-turn rectangular solenoid utilized in our wide bore ^{1}H–^{15}N 600 MHz probe has an inner cross section of 8×6 mm and is roughly 12 mm in length or $\sim 580\ mm^3$ in volume (Fig. 1C). The freestanding coil is constructed from thin copper strip (0.25×2.0 mm, C10100 hard temper copper, MWS Wire Industries, Westlake Village, CA) in order to maximize filling factor. The wide copper strip reduces gaps between the turns and limits RF inhomogeneity in the proximity of these gaps. A hard-tempered copper strip grade is used to better maintain coil shape and plastic reinforcement plates are affixed to the top and bottom planes of the coil by drops of low-loss epoxy in order to avoid deformation by a careless user. The material for these reinforcement plates (Rexolite™, Boedeker Plastics Inc., Shiner, TX), and the drops of epoxy (EPO-TEK H54 insulating epoxy, Epoxy Technology Inc., Billerica, MA) that attach plates to the copper windings were chosen for their small dielectric constant and low dielectric loss tangent at high frequencies. The sample coil is thermally insulated inside a Teflon variable-temperature chamber and is detachable by means of two brass screws that mount it to copper posts (Fig. 1C) leading to the RF circuit situated below the chamber (Fig. 1B). This allows quick and solderless switching between sample coils of varying sizes and geometries as long as their inductance values are similar.

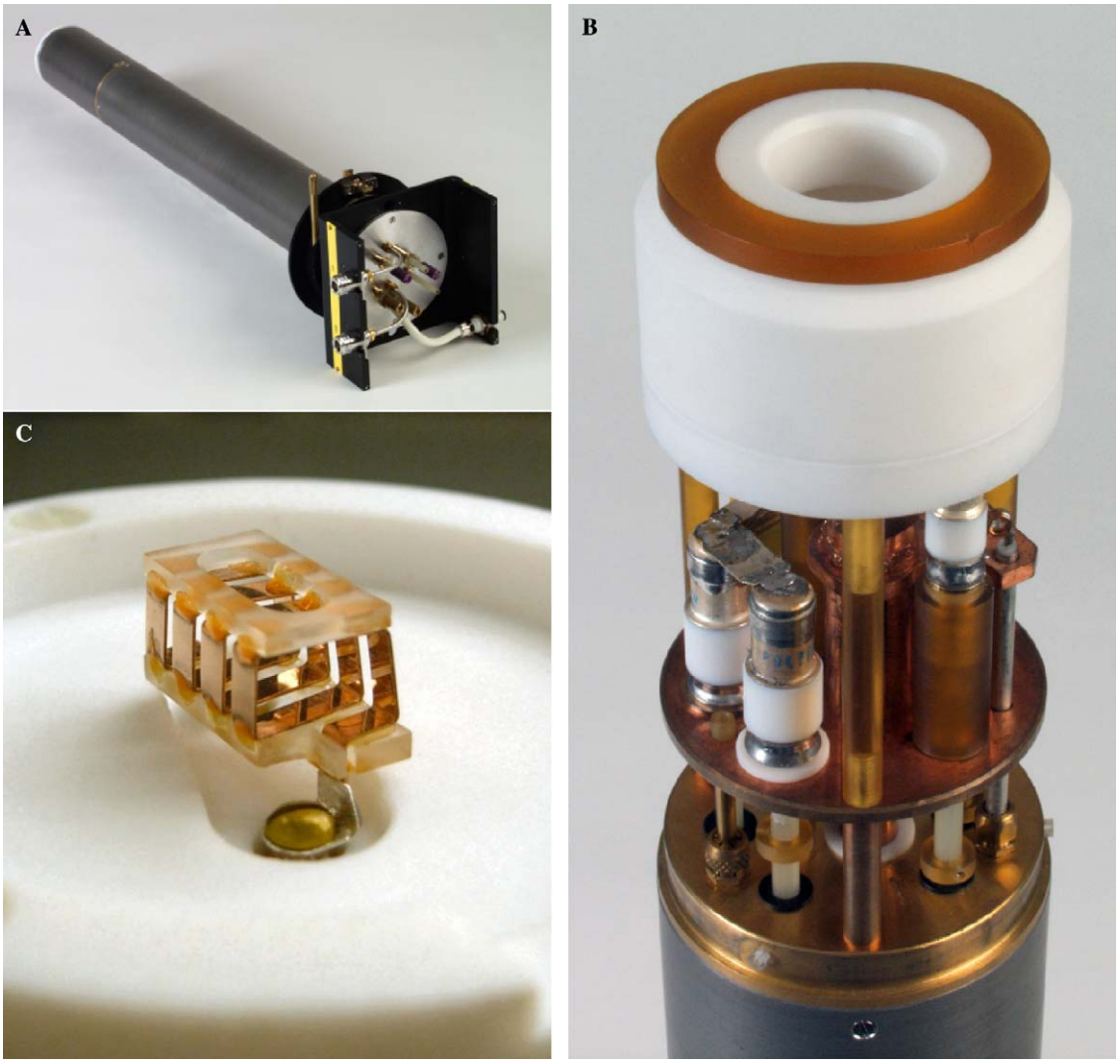

Fig. 1. (A) Photograph of the probe; (B) probehead view showing Teflon variable temperature chamber with a hole for interfacing an upper VT stack; (C) close up of interchangeable flat sample coil inside the VT chamber.

To save valuable probehead space for large high voltage matching components, the temperature control for the sample is maintained by an airflow through an external home-built upper VT stack, sealed to the probe by a silicone O-ring. Long-term temperature stability is achieved between −40 and +100 °C, which is sufficient for most experiments on biological solids. The RF circuitry is ventilated by a separate stream of room temperature air to prevent a rise in reflected power from the heating of individual components during long, high power pulse trains.

2.2. Probe RF circuit

While the efficiency of the low-frequency ^{15}N channel benefits from the higher turn density in the sample solenoid, too many turns, on the other hand, tend to destroy RF field homogeneity of the ^{1}H channel and complicate the CP experiment. Still, because low ^{15}N sensitivity is always a concern, the sample coil is wound with as many turns as possible such that its electrical length does not dramatically exceed $1/4\lambda$ at the ^{1}H frequency, with resulting ^{1}H inhomogeneity corrected in the circuit design stage. The 4-turn coil implemented in this probe corresponds to $\approx 0.27\lambda$ in air at 600 MHz (including leads passing through the VT chamber dielectric) and has an inductance value of 80 nH.

Wavelength effects in a $1/4\lambda$ unbalanced solenoid seriously degrade the homogeneity of the RF field at ^{1}H frequency [13,19,20]. The current distribution has its peak at the grounded end and its minimum at the driven end of the coil. This leads to a B_1 profile skewed towards the grounded side of the solenoid, jeopardizing the quality of cross-polarization experiments. Such adverse effects are reduced by electrically balancing the sample coil [20,21,13], i.e., by terminating the coil leads with equal impedance to ground. In a balanced arrangement, the voltage node is moved to the middle of the coil, essentially dividing the long sample coil into two shorter, grounded, series-connected coils. The current is forced to peak at the center of the solenoid and decrease symmetrically

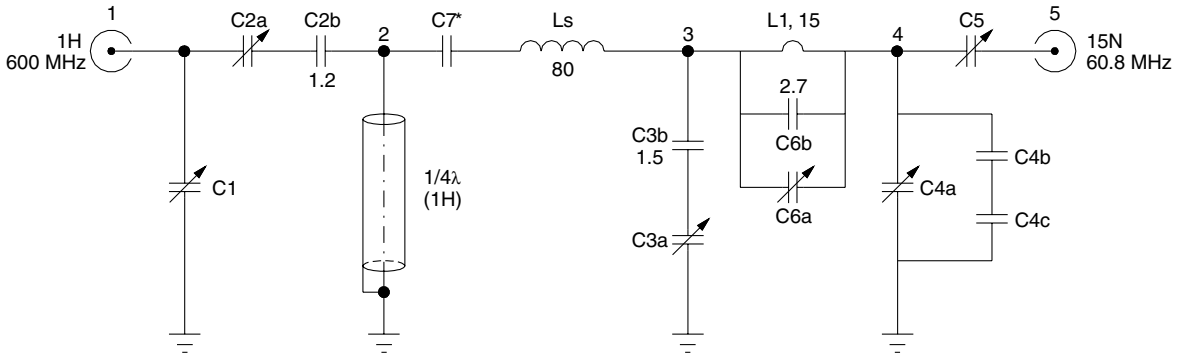

Fig. 2. Electrical schematic of the 600 MHz large sample ^{1}H–^{15}N flat coil probe. C_1, C_{2a}, and C_{3a} provide matching, tuning, and balancing for the ^{1}H channel (600 MHz), respectively. C_{4a} and C_5 tune and match the lower frequency ^{15}N channel (61 MHz). Optional fixed symmetry capacitance C_7 balances the coil at the low frequency to reduce voltage at nodes 4 and 3 on the right side of the circuit. Shown component values are in pF and nH.

toward the ends, greatly improving the B_1 distribution in the coil. Also, the maximum voltage to ground is halved, reducing high-voltage requirements on the components in the adjacent matching network.

Fig. 2 shows the dual-balanced version of a double-tuned CHW circuit employed in our 600 MHz ^{1}H–^{15}N probe. The $1/4\lambda$, shorted coaxial trap provides high impedance for the ^{1}H signal and a ground path for the ^{15}N signal, while the parallel trap L_1-C_6 is tuned to the vicinity of 600 MHz for high impedance and reflection of the ^{1}H signal. The ends of the sample coil, *Ls*, are balanced with respect to ground at both frequencies. At the ^{1}H frequency, the impedance at the ends of the coil is balanced by adjusting the ratio of the symmetry capacitance C_3 to the tuning capacitance C_2. Adjustment of the ^{1}H matching capacitor C_1 does not disturb the coil balance because $C_1 > 4C_2$ and the voltage at node 1 is negligible compared to that at node 2. Placing the matching capacitor between node 1 and ground [22,23] instead of the more common inline approach allows use of a smaller, lower voltage trimmer (NMKT series from Voltronics Corp., Denville, NJ) and allows the ^{1}H channel to be tuned to higher frequency. Capacitors C_{4a} and C_5 that tune and match the nitrogen channel are high-voltage variable trimmers (Polyflon Co., Norwalk, CT, model RP-VC5-10). The sample coil is balanced at the ^{15}N frequency by fixed symmetry capacitance C_7 to reduce the voltage on nitrogen trimmer C_{4a}. Capacitance C_7 does reduce the tuning range of the ^{15}N channel by requiring larger values of $C_{4a} + C_{4b}$, and can be omitted unless especially large B_1 values are sought. Other variable capacitors in the circuit (C_{2a}, C_{3a}, and C_{6a}) are the smaller 0.3 to 3 pF Polyflon model RP-VC3-6, which were chosen for having self-resonance frequencies higher than 600 MHz. The use of larger variable capacitors with lower self-resonant frequencies, which change with piston position, can place an effective LC "short" in the vicinity of the ^{1}H frequency, making ^{1}H circuit tuning and balancing practically impossible.

Proper circuit balancing can be established at both frequencies by touching the RF solenoid at different points along its length with a sharpened, grounded wire and observing the changes in frequency or matching condition of the probe resonance with a reflection bridge or vector network analyzer (VNA). The point of maximum current in the coil is a zero-voltage node—a virtual ground. Touching the RF coil at that point with a grounded wire will produce no change in the resonance curve. At all other points along the coil, some current will be diverted into the wire, resulting in a shift and/or mismatch of the resonance. Scanning the coil with the grounded wire determines the initial location of the virtual ground node. The symmetry capacitance can then be adjusted until the node is close to the middle of the RF coil, at which point the probe is well balanced.

2.3. Isolation traps

From the standpoint of ^{15}N, inductor L_1 in the high-frequency reflection trap L_1-C_6 is effectively in series with the sample coil *Ls*. The ^{15}N efficiency is therefore enhanced by using the smallest possible inductor L_1. We used a 1/2-turn inductor made of 2.5 mm thick Cu wire with a radius of ≈6 mm and an inductance value of ≈15 nH. The capacitance C_6 consists of a trimmer and fixed capacitor in parallel to achieve the required voltage and capacitance in the available space. The fixed capacitance C_{6a} can be one of the larger case, high-voltage multilayer ceramic chip capacitors (100C or 100E series from American Technical Ceramics, 25 or 38 series from Dielectric Lab sold by Voltronics Corp.) that will withstand the high ^{1}H voltage experienced by this trap. Unfortunately, with a chip capacitor this reflection trap produced an unacceptable level of ringing in the ^{15}N channel. To reduce the ringing, we constructed a 2.7 pF tubular capacitor C_{6a}, made of two concentric Cu conductors with PTFE dielectric in between. The edges of the outer tube are carefully rounded off to avoid arcing. In order to compare the quality of the traps with the tubular and chip capacitors, Q-measurements for the isolated L_1-C_6 trap assemblies were made using the VNA and a probing loop. The trap with the tubular capacitor yielded an *unloaded* Q of 520, while the traps made with chip capacitors had unloaded Q's in the range of 400–430.

Because the impedance of the L_1-C_6 trap at resonance is given by

$$Z_{LC} = Q_{LC}\omega L_1 = Q_{LC}\frac{1}{\omega C_6}, \quad (1)$$

where Q_{LC} is the unloaded Q of the entire trap, increasing the trap Q can be expected to improve the ^{1}H channel efficiency. And since we employ the smallest possible L_1 to reduce loss in the ^{15}N channel, the higher Q should partially offset the effect of the small inductance.

It has been observed that losses in transmission line traps can lead to poor efficiency in double tuned probe circuits [11]. Therefore, seven shorted coaxial line traps of varying designs (Fig. 3) were tested to find the best performance. One trap was made from commercial, large diameter semi-rigid coaxial cable (UT-390, Microstock Inc., West Point, PA) and the rest were custom made. All traps, including the one fabricated from UT-390, consist of an outer conductor tube of 10 mm OD and 8.4 mm ID. When choosing the tube for the outer conductor there exists a variety of thin wall copper tubing commercially available in this size range. Our experience, however, suggests that they are most often made of UNS C12200 copper, an alloy designed for welding and solder applications with 20% lower conductivity than that of electrical grade copper such as alloys C10100, C10200, and C11000 [24]. To reduce resistive losses in the custom traps, we machined both the outer and inner conductors from the C10100 grade solid rod. Each inner conductor rod has a 2–56 threaded hole cut into both ends. In traps with small inner conductor, a short stub with a threaded hole was soldered at each end of the wire. To ground one end of the trap, the end cap is pressed onto the outer tube and the inner rod is attached with a screw and tightened with a split lock-washer. For air-dielectric traps, a short PTFE spacer is used to center the inner conductor at the open end of the tube. Otherwise, a continuous dielectric tube is inserted between the outer and inner conductor. The trap assembly is installed with the help of the custom compression clamps (Fig. 3) threaded into the frame of the probe. To minimize stray leads, the exposed part of the inner conductor rod with a threaded hole in it, serves as one of the mounting posts for the sample coil. Use of clamps and screws instead of solder connections allowed for easier swapping of coaxial traps during the optimization process described further below.

Fig. 3. A shorted coaxial trap of air dielectric is shown with a compression clamp that mounts it inside the probe. Another coaxial trap with a 99.9% Al_2O_3 dielectric is shown to the right.

2.4. Circuit losses from double tuning the network

The loss associated with double tuning the probe occurs in the reflection trap L_1-C_6 and in the shorted coaxial stub. In order to determine how much loss is contributed by each trap, we removed them from the circuit in turn by shorting or disconnecting as appropriate and measured changes in the performance of both channels. To obtain meaningful results for the ^{1}H channel, it is necessary to maintain the same v/B_1 (Volts per kHz of B_1 field) across each trap following each circuit modification. This condition is achieved by readjusting the electrical balance of the sample coil using the procedure outlined above. It was not necessary to balance the coil for ^{15}N measurements since the inductive elements of both traps, which at low frequency are responsible for nearly all the RF loss, are in series with the sample coil. The coaxial trap used here was made from UT-390 semi-rigid coaxial cable, with inner conductor diameter of 2.6 mm, and characteristic impedance $Z_0 = 50\ \Omega$. Table 1 shows the RF power required to generate same B_1 field magnitude in the double-resonance circuit (Fig. 2) and in the single-resonant circuits where one or both traps are eliminated.

To check for consistency, we take the power needed to generate 100 kHz in the simplest ^{1}H circuit with both traps removed as a reference (line 1 in Table 1). To generate 100 kHz B_1 in other configurations one needs to add extra power on top of that (second column). The sum of additional power from lines 2 and 3 should be roughly equal to that for the complete circuit in line 4, and the agreement is within ~10%. This is in good agreement considering that balancing of the coil with a ground wire is not a very accurate procedure. Similarly for ^{15}N frequency losses, the sum of additional power in lines 6 and 7 is in good agreement with line 8.

Table 1
Measurement of RF loss in the coaxial and LC trap

^{1}H configuration:	$B_1 = 100$ kHz power, W	Extra power (W)
1. Both traps removed	47	—
2. L_1-C_6; 1/4λ coax removed	169	+122
3. 1/4λ coax; L_1-C_6 removed	108	+61
4. Complete ^{1}H circuit	214	+167
^{15}N configuration:	$B_1 = 50$ kHz power, W	Extra power (W)
5. Both traps shorted	448	—
6. L_1-C_6; 1/4λ coax shorted	494	+46
7. 1/4λ coax; L_1-C_6 shorted	619	+171
8. Complete ^{15}N circuit	672	+224

Measurements performed with 100% neutral paraffinic oil and ^{15}N-labeled $(NH_4)_2SO_4$ crystalline powder for ^{1}H and ^{15}N frequencies, respectively.

Table 1 shows that the ^{1}H field of 100 kHz can be achieved with only 214 W, which is less than our budget of 300 W. Since our goal is to achieve the best ^{15}N efficiency consistent with the required ^{1}H B_1 field, we can investigate the possibility of reducing ^{15}N loss in the coaxial trap even at the expense of some further loss in ^{1}H efficiency. The dominant source of loss in the ^{15}N observe channel is the UT-390 coaxial trap, which increases the power required by almost 40% compared to only 10% added by L_1. We can therefore ask how to modify the coaxial trap to reduce its loss for the ^{15}N channel while staying within our ^{1}H efficiency specification.

2.5. Analysis of losses in coaxial λ/4 trap at ^{1}H and ^{15}N frequency

We consider first loss in the shorted coaxial trap at the high ^{1}H frequency. The RF energy reaching the sample coil is maximized for a trap having the highest possible input impedance. The impedance $Z_{\rm in}$ of a shorted transmission line is

$$Z_{\rm in} = Z_0 \tanh \gamma l, \tag{2}$$

where Z_0 is the characteristic impedance of the line, l is the length of the line, and γ is the propagation constant $\gamma = \alpha + j\beta$ [25]. Since $\beta = 2\pi/\lambda$ and $l = \lambda/4$, we obtain for a low-loss line

$$Z_{\rm in} = Z_0 \tanh\left(\alpha l + j\frac{\pi}{2}\right) = Z_0 \coth(\alpha l) = Z_0\left(\frac{1}{\alpha l} + \frac{\alpha l}{3} + \cdots\right) \approx \frac{Z_0}{\alpha l} = \frac{4f\sqrt{\mu\varepsilon}Z_0}{\alpha}, \tag{3}$$

where ε is the dielectric constant and μ is the permeability of the dielectric. For the present purposes, it is useful to replace attenuation coefficient α by the physical parameters of the transmission line. Again from [25]

$$\alpha = \frac{R}{2Z_0} + \frac{GZ_0}{2}, \quad \text{where } R = \frac{R_S\sqrt{f}}{\pi}\left(\frac{1}{d_o} + \frac{1}{d_i}\right), \tag{4}$$

R and G are the distributed resistance and conductance per unit length, R_S is the skin effect surface resistivity in units of $\Omega/\mathrm{Hz}^{1/2}$, d_i and d_o are the inner and outer diameters of the dielectric, and f is the frequency. We assume that G can be neglected at NMR frequencies. We will also need the characteristic impedance in terms of the physical parameters

$$Z_0 = \frac{1}{2\pi}\sqrt{\frac{\mu}{\varepsilon}}\ln\left(\frac{d_o}{d_i}\right). \tag{5}$$

Substituting (4) and (5) into (3), the input impedance can be expressed as

$$Z_{\rm in} = \frac{2d_o\sqrt{f}}{\pi R_S}\sqrt{\frac{\mu^3}{\varepsilon}}\frac{(\ln g)^2}{1+g}, \quad \text{where } g = d_o/d_i. \tag{6}$$

This expression summarizes the relevant scaling for the input impedance of a shorted 1/4λ trap at resonance. An ideal trap would have infinite $Z_{\rm in}$. Not surprisingly, we can improve a trap by increasing its diameter d_o or by decreasing the resistivity R_S. Lowering the dielectric constant ε also increases $Z_{\rm in}$. Increasing the permeability is almost certainly not a practical alternative in an NMR magnet. These factors are all independent of g, the ratio of outer to inner diameter. One can show by differentiating Eq. (6) that $Z_{\rm in}$ is maximized at $g = 9.19$. This is not the value $g = 3.59$ that minimizes attenuation of a traveling wave α and is used to design air-dielectric coaxial lines of 75 Ω and PTFE cables of 50 Ω. The ratio 9.19:1 produces a transmission line with an impedance of 133 Ω for an air dielectric. Fig. 4A illustrates the dependence of α and $Z_{\rm in}$ on g. A transmission line with $g = 3.59$ has an input impedance 74% that of an optimized trap. It is interesting to note how rapidly $Z_{\rm in}$ decreases for small values of g. As $d_o \to d_i$, the trap will perform very poorly.

In a CHW style probe, the shorted 1/4λ coax functions as a low-frequency "short" to ground at the same time as it is nearly an open circuit for ^{1}H. At ^{15}N, the coax is a "λ/40" stub, connected in series to the sample coil. The wavelength effects can therefore be neglected. The series resistance rather than the attenuation coefficient determines the trap's efficiency at the ^{15}N frequency f_x. In this regime, the resistance of the "short" is

$$R_{\rm in} = Rl = \frac{R_S l\sqrt{f_X}}{\pi}\left(\frac{1}{d_i} + \frac{1}{d_o}\right), \tag{7}$$

where R is the resistance per unit length. The length l depends on the wavelength for the ^{1}H frequency in the trap, so we can write it as

$$R_{\rm in} = \frac{R_S(g+1)}{4\pi d_o A\sqrt{f_X\mu\varepsilon}} = 2\alpha l Z_0, \tag{8}$$

where $A = \gamma(^1H)/\gamma(X)$ is the ratio between the gyromagnetic ratio of the nuclides. Not surprisingly, as the outer radius increases or the resistivity decreases, the stub's resistance decreases. Increasing either the frequency or the dielectric constant will shorten the line and reduce $R_{\rm in}$. While large values of permeability μ would make for a very efficient probe at both frequencies, this is, unfortunately, hardly practical for NMR purposes. The plot in Fig. 4B illustrates

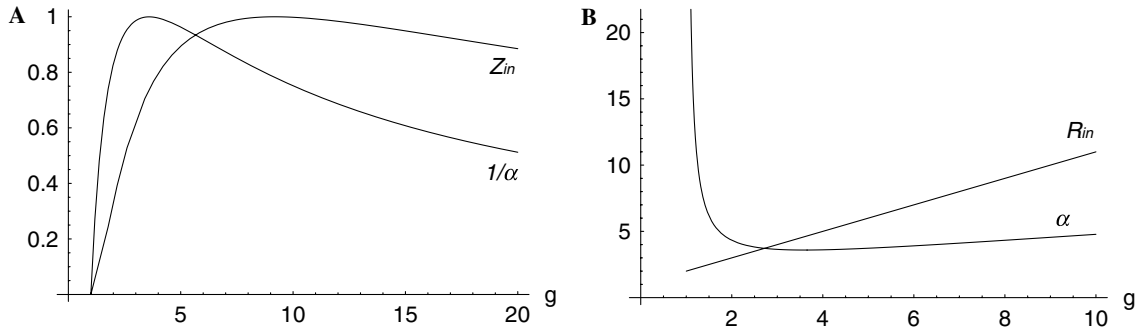

Fig. 4. (A) A normalized plot of the high-frequency impedance Z_{in} of the shorted coaxial 1/4λ trap with its inverse attenuation coefficient, as a function of $g = d_0/d_i$; (B) low-frequency resistance R_{in} of the shorted coaxial 1/4λ trap and its attenuation coefficient, as a function of $g = d_0/d_i$.

the difference in the dependence of R_{in} and the attenuation coefficient α. While α has a definite minimum for $g = 3.59$, R_{in} simply increases linearly with g. In neither the resonant nor the low frequency case does the attenuation coefficient α alone provide a useful measure of the quality of the coaxial trap for the present purposes.

2.6. Optimization of the $\lambda/4$ coaxial trap

Based on the analysis above, the ideal 1/4λ trap would consist of coaxial air-line with as large an inner conductor as possible for ^{15}N efficiency and with the g ratio set to 9.19 for ^{1}H efficiency. Unfortunately, it is not possible to meet both conditions in the limited space available inside the probehead. In our 600 MHz flat coil probe the coaxial trap outer diameter was mechanically constrained to a 10 mm clearance in the compression clamp, allowing for a maximum dielectric OD of $d_o = 8.4$ mm. Making the best use of power available to each channel should also be considered. Our present aim is to produce a 100 kHz B_1 field at ^{1}H and at least 50 kHz B_1 field at ^{15}N frequency, using 300 W and 1 kW amplifiers, respectively. Several traps of different dielectric materials and Z_0 values were constructed with the aim of achieving the best ^{15}N sensitivity while producing the required ^{1}H B_1, and NMR measurements of B_1 field strength were obtained for each trap installation. 100% neutral parafinic oil was used to measure ^{1}H 90° pulses and ^{15}N-labeled $(NH_4)_2SO_4$ crystalline powder was used to track changes in ^{15}N channel efficiency. The results are summarized in Fig. 5 and Table 2. Values given for Z_0, Z_{in} and R_{in} were calculated from physical parameters while ^{1}H and ^{15}N B_1 field strengths were measured by NMR at fixed power levels (66 W for ^{1}H and 700 W for ^{15}N) and then extrapolated to yield RF power required to reach the target fields.

Fig. 5A shows that the measured ^{15}N 90° pulse length $(\tau_{90})^2$ has the expected linear dependence on the calculated trap resistance R_{in}. Extrapolating the linear fit to its y-intercept at $R_{in} = 0$ illustrates the performance τ_{90min} that would be achieved with an ideal, lossless coaxial stub. For ^{15}N, it is 3.8 μs at 700 W input power. Because the trap resistance R_{in} is in series with the resistance of other elements in the circuit (sample coil, inductor L_1, resistance of leads), the x-intercept of the fit yields the effective resistance R_{eff} contributed by the rest of the circuit, in this case $R_{eff} \approx 0.40\ \Omega$. A similar analysis can be applied to the ^{1}H 90° pulse data. Because in the ^{1}H circuit the trap impedance Z_{in} is parallel to the impedance Z_{eff} of the sample coil and the parallel trap, it is easier to work with the trap admittance, defined as $Y_{in} = 1/Z_{in}$. As shown by Fig. 5B, an improvement of ^{1}H efficiency by the coaxial trap is limited to $\tau_{90min} = 3.9$ μs at 66 W input power. The effective impedance Z_{eff} of the rest of the ^{1}H circuit is ≈20 kΩ at 600 MHz. We can also compare the values τ_{90min} determined from the y-intercepts in Fig. 5 with the τ_{90} values in Table 1 since the removal of the 1/4λ trap from each channel should produce an effect identical to the use of a lossless trap. Fig. 5B illustrates that the value from Table 1 is in reasonable agreement with the extrapolated τ_{90min} for the ^{1}H channel. The measured ^{15}N τ_{90} from Table 1 is somewhat larger than the extrapolated value in Fig. 5A, probably due to the finite impedance of the short used to ground the coaxial trap at node 2 of Fig. 2.

Trap efficiency at the ^{1}H frequency does indeed reach its optimum in the vicinity of $Z_0 \sim 130\ \Omega$, as predicted. A 130 Ω trap would be optimal for a double-tuned probe having a less important low-frequency channel such as a field-frequency lock. With 300 ^{1}H and 1 kW ^{15}N amplifiers, only two of the traps in Table 2 are able to achieve target fields of 100 and 50 kHz, respectively. Better ^{15}N efficiency is always a primary concern for our membrane protein application, and with 300 W of available ^{1}H power, the practical compromise was made in favor of using air-filled trap #3 with 4.8 mm inner conductor diameter and Z_0 of 34 Ω.

As the electrical length of the solenoid exceeds 1/4λ at the ^{1}H frequency, its reactance changes sign from positive (inductance) to negative (capacitance), and it can no longer be tuned with only capacitive elements. Reducing the coaxial trap length to <0.25λ adds a positive reactance in parallel with the negative reactance of the sample coil Ls, and thus increases the tuning limit to a higher frequency. For this reason, all the shorted 1/4λ traps discussed in this article are actually 0.225λ. In fact, we were able to employ traps as short as 0.210λ without a detectable change in

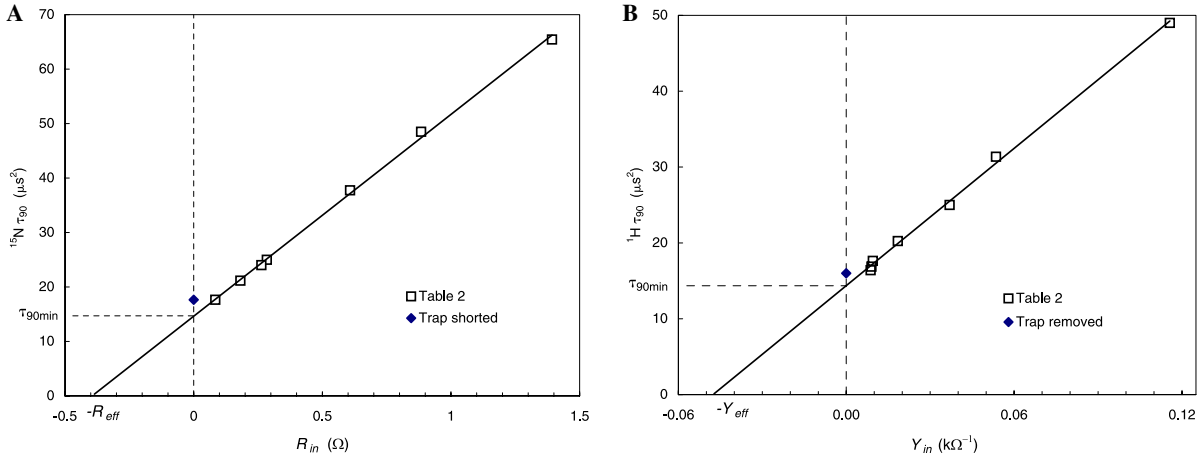

Fig. 5. (A) Linearized plot of the ^{15}N efficiency of the shorted 1/4λ coaxial trap as a function of series resistance R_{in}; (B) linearized plot of the ^{1}H efficiency of the shorted 1/4λ coaxial trap as a function of its admittance $Y_{in} = 1/Z_{in}$.

Table 2
Power efficiency of ^{1}H and ^{15}N channels for different 1/4λ coaxial traps

Trap dielectric	ε_r	d_i (mm)	$g = d_0/d_i$	Z_0 (Ω)	Z_{in} (kΩ)	^{1}H $B_1 = 100$ kHz W	R_{in} (Ω)	^{15}N$B_1 = 50$ kHz W
1. 99.9% alumina	9.8	4.8	1.8	11	9	517[a]	0.08	471
2. PTFE	2.1	4.8	1.8	23	19	331[a]	0.18	567
3. Air line	1.0	4.8	1.8	34	27	265	0.26	645
4. PTFE, UT-390	2.03	2.6	3.2	50	55	214	0.28	672
5. Air line	1.0	1.57	5.4	101	106	186	0.60	1008[a]
6. Air line	1.0	1.02	8.3	127	115	173	0.89	1295[a]
7. Air line	1.0	0.62	14	156	111	178	1.39	1747[a]

RF power levels required to achieve ^{1}H B_1 fields of 100 kHz and ^{15}N B_1 fields of 50 kHz, are shown in Watts. Traps sorted by Z_0 value, $d_o = 8.4$ mm for all traps, $\varepsilon_r = \varepsilon/\varepsilon_0$ is the dielectric constant relative to that of free space.

[a] Beyond power limit of amplifier.

the ^{1}H 90° pulse length. The τ_{90} became progressively longer for traps $<0.210\lambda$.

2.7. Sample preparation

The transmembrane domain SSDP[L$_{26}$-^{15}N]VVAASII-GI[L$_{36}$-^{15}N]H[L$_{38}$-^{15}N]I[L$_{40}$-^{15}N]WI[L$_{43}$-^{15}N]DRL of the M2 protein (M2 TMD) from influenza A virus [7] was prepared by solid-phase peptide synthesis and co-dissolved in trifluoroethanol (TFE) with 1,2-dimyristoyl-*sn*-glycero-3-phosphatidyl-choline (DMPC) in a 1:16 molar ratio. The carboxyamidated single site ^{15}N-labeled piscidin-1 sample (NH$_2$-FFHHIFRGIVHVGKT[I-^{13}C′]HRL[V-^{15}N]TG-NH$_2$) of an antimicrobial peptide from mast cells of fish [18] was prepared by solid-phase peptide synthesis and dissolved in water, while the lipids, DMPC and 1,2-dimyristoyl-*sn*-glycero-3-phospho-rac-(1-glycerol) (DMPG) in a 4:1 molar ratio, were dissolved separately in chloroform. The solutions were combined to achieve a 1:20 peptide-to-lipid molar ratio and methanol was added to achieve a single transparent phase. The solvent was removed by a rotary evaporator in both peptide containing samples followed by drying under vacuum overnight. The lipid film was rehydrated with a buffer (pH 6), forming multilamellar liposomes containing the peptide material. The liposomes were then pelleted by ultracentrifugation at 104,000g. The pellets were collected and deposited on thin, 30 μm, 5.7 × 12.0 mm glass slides (Matsunami Trading Co., Ltd., Osaka, Japan) and allowed to dehydrate at 98% relative humidity and room temperature. The slides were rehydrated to reach 50% hydration by weight, stacked and then sealed with bees-wax (Hampton Research, Aliso Viejo, CA) in a rectangular sample cell (Vitrocom Inc., Mountain Lakes, NJ) to maintain a constant hydration level during incubation (1 day at 43 °C) and during the NMR experiments (Fig. 6).

3. Results

3.1. RF Performance

RF performance of the 600 MHz large volume ^{1}H–^{15}N flat coil probe is summarized in Table 3. The 8 × 6 × 12 mm flat coil was measured to deliver ^{1}H peak fields of 100 kHz in a non-lossy paraffinic oil sample with 265 W of input power. At the ^{15}N observe frequency (61 MHz), 700 W of input power produced peak fields of 54 kHz in *N*-Acetyl-^{15}N-valine single crystal. These B_1 fields can be sustained for at least 5 ms in each channel simultaneously, without arcing. Isolation between channels is $\geqslant 25$ dB at both ^{1}H and ^{15}N resonances. Figs. 7A and B show B_1 nutation profiles obtained at both frequencies over

Fig. 6. Typical size of a sample cell used in our laboratory. The US 10¢ coin is shown underneath for scale reference.

Table 3
Performance of large sample ^{1}H–^{15}N probe at 600 MHz

Channel (MHz)	Power (W)	B_1 (kHz)	Isolation (dB)	B_1 homogeneity ($A_{810°}/A_{90°}$)
^{1}H, 600	265	100	25	71%
^{15}N, 61	700	54	28	76%

Trap #3 is used. The RF coil volume is $8 \times 6 \times 12$ mm or ~580 μL. Peak RF fields are sustainable for at least 5 ms without arcing.

$6 \times 4 \times 9$ mm rectangular reference samples centered in the coil.

Electrical balancing of the sample coil is expected to improve the B_1 homogeneity in the ^{1}H channel. The extent of improvement could, in principle, be evaluated by measuring the B_1 nutation profile in a deliberately unbalanced circuit, grounded at node 3. However, because the electrical length of the coil is $>1/4\lambda$ at 600 MHz, this probe could not be tuned to that frequency in an unbalanced mode. Instead, we obtained an RF homogeneity measurement with the same sample coil and a similar RF circuit in a 400 MHz spectrometer (Fig. 7C). The wavelength effects for this size solenoid are already very significant at 400 MHz—the $A_{810°}/A_{90°}$ ratio is only 27% for the unbalanced coil. The inhomogeneity would be even worse at 600 MHz.

Initially, we encountered ringing at the ^{15}N frequency exceeding 200 μs. Replacing C_{6b} with the custom tubular capacitor reduced the ring-down time to approximately 100 μs. The ringing capacitors were identified by sequential elimination, and were then placed at different orientations to the magnetic field until the ring-down was reduced to less than 20 μs. The best orientation found for 100C series chip capacitors was where both the flat side and solder plates are parallel with the magnetic field. The extent to which re-orientation helps reduce ringing seems to be a function of the individual batch of capacitors. Capacitors from some batches continued ringing regardless of orientation and could not be used.

It is important to note that the ^{1}H channel efficiency varies from one oriented sample preparation to another depending on sample salinity and hydration levels. This is attributable to RF heating caused by lossy samples interacting with electric fields inside the RF solenoid. At the ^{1}H frequency, these RF losses take away from the B_1 field produced by the coil. The resultant decoupler heating causes a loss of hydration in some of the samples resulting in their heterogeneity and instability during long-term experiments [26]. Hydration loss manifested itself by tiny water droplets that formed on the inner surface of glass sample cells. Decoupling fields and/or duty cycle for such samples had to be reduced to stabilize the sample.

3.2. PISEMA Capabilities

Experimental ^{15}N PISEMA capabilities of the flat coil probe are demonstrated in Figs. 8 and 9. Both experiments were conducted using a Bruker 600 MHz (14.1 T) wide bore spectrometer. In both cases, the minimum B_1 sufficient for the sample under study was used to avoid heating and damaging the sample. An ^{15}N PISEMA spectrum of five site ^{15}N-$Leu_{26,36,38,40,43}$-M2-TMD oriented in DMPC bilayers was recorded in the presence of 10 mM amantadine (Fig. 8). While two of the five resonances appear to be overlapping the spectral resolution is excellent, especially considering the dynamics that this protein displays in the transmembrane region [28]. Even without resonance assignments it is clear that the helical tilt is very different from that observed in the absence of amantadine. Here, the tilt angle appears at least 10° less than the $37 \pm 3°$ observed in the absence of amantadine. Other high-resolution 2D NMR spectra of M2 TMD aligned both by glass support and by a novel approach utilizing nanoporous anodic aluminum oxide substrate have been obtained using this 600 MHz probe and reported earlier [29]. Fig. 9 shows the 2D ^{15}N–^{1}H PISEMA spectrum obtained from a single site ^{15}N-labeled piscidin-1 sample (NH_2-FFHHIFRGIVHVGKT[I-$^{13}C'$]HRL[V-^{15}N]TG-NH_2), an antimicrobial peptide from mast cells of fish. This sample preparation was unusual in terms of internal RF losses, producing a 50% drop in ^{1}H B_1 field upon sample insertion—the largest we have ever experienced. However, this spectrum shows a 5 ppm linewidth in the chemical shift and a 600 Hz linewidth in the dipolar dimension. The resonance frequencies suggest that the helical structure is in an orientation approximately perpendicular to the bilayer normal.

4. Discussion and conclusion

The design and application of a 600 MHz, 580 mm^3 flat coil ^{15}N–^{1}H solid-state NMR probe for oriented membrane proteins has been demonstrated. The high field probe accommodates large volumes of dilute sample while employing RF solenoids with electrical lengths greater than $1/4\lambda$ at the ^{1}H frequency to enhance ^{15}N sensitivity. ^{1}H RF

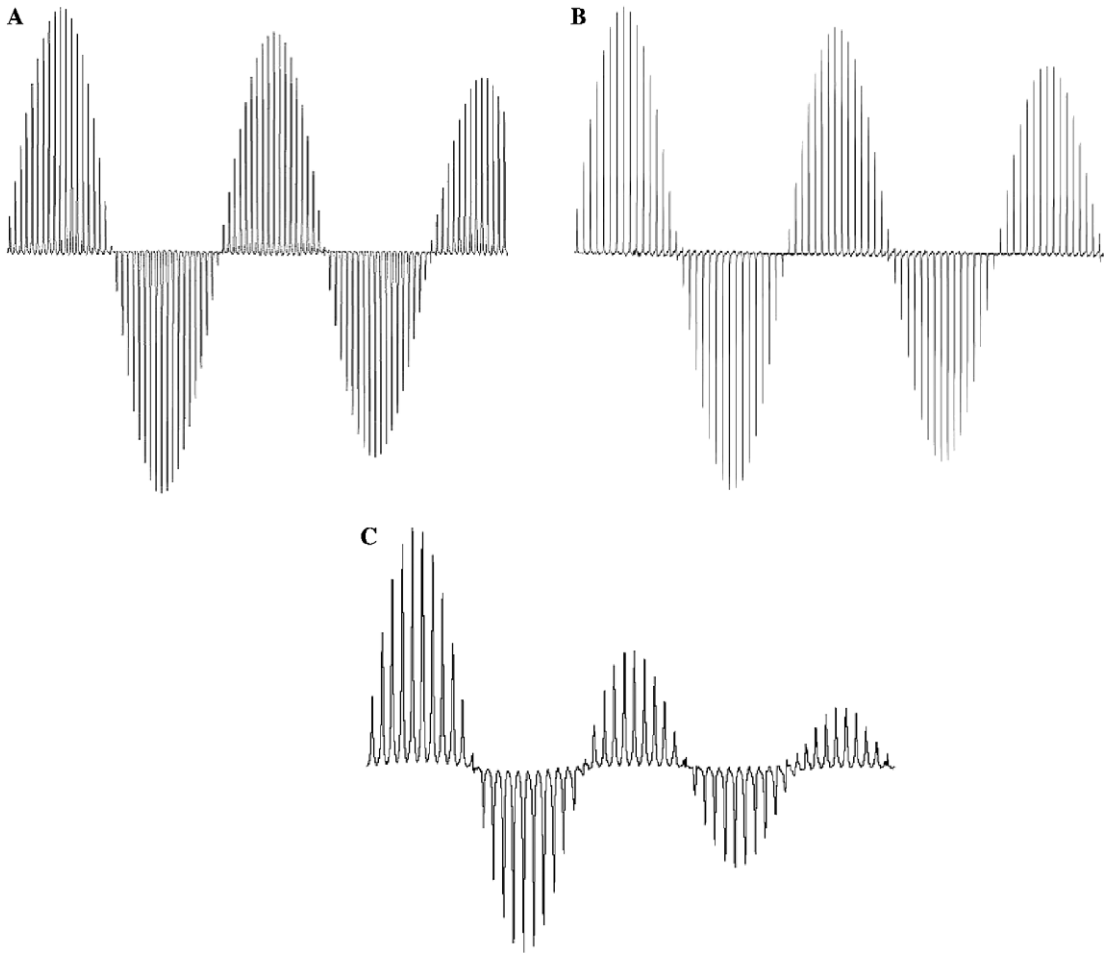

Fig. 7. B_1 nutation profiles across $4 \times 6 \times 9$ mm rectangular reference samples: (A) 600 MHz, ^{1}H channel, $A_{810°}/A_{90°} = 71\%$; (B) 61 MHz, ^{15}N channel, $A_{810°}/A_{90°} = 76\%$; (C) deliberately unbalanced ^{1}H channel at 400 MHz, $A_{810°}/A_{90°} = 27\%$.

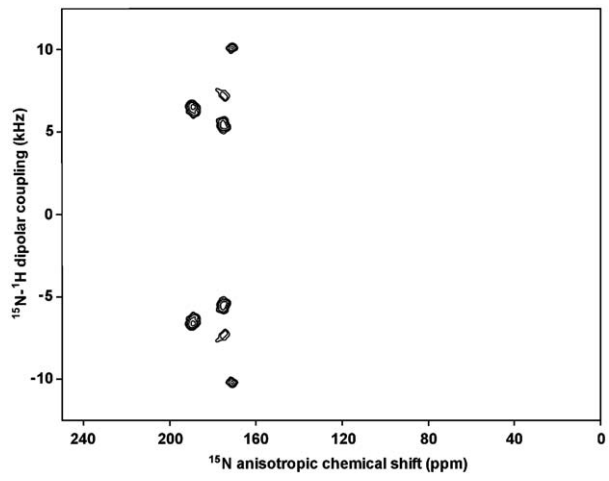

Fig. 8. 600 MHz 2D ^{15}N–^{1}H PISEMA spectrum of 8 mg ^{15}N-Leu$_{26,36,38,40,43}$-M2-TMD oriented in DMPC in the presence of 10 mM amantadine. Experimental parameters: 8 mg of the M2-TMD, the line widths are 700 Hz along the dipolar dimension and 8 ppm along the chemical shift axis, 64 t_1 increments with 128 transients each, 6 s recycle delay, B_1 ^{1}H (decoupling) = 36 kHz, B_1 cross-polarization = 40 kHz, Lee–Goldburg = 30 kHz, sample temperature 25 °C, total acquisition time 13.6 h. The dipolar axis is adjusted to account for the scaling factor of 0.81 arising from the application of phase-alternated Lee–Goldburg homonuclear decoupling [27,6].

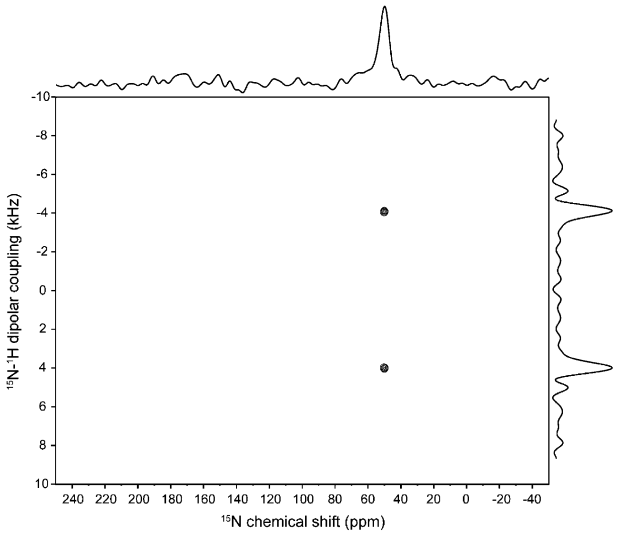

Fig. 9. 2D ^{15}N–^{1}H PISEMA spectrum of a single site ^{15}N-labeled piscidin-1 sample (NH_2-FFHHIFRGIVHVGKT[I-^{13}C′]HRL[V-^{15}N]TG-COOH) at 600 MHz. Experimental parameters: 12 mg of amidated piscidin-1, 24 t_1 increments with 288 transients each, 6 s recycle delay, B_1 ^{1}H (decoupling) = 30 kHz, B_1 cross-polarization = 30 kHz, Lee–Goldburg = 22 kHz, sample temperature 36 °C, total acquisition time 11.5 h. The dipolar axis is adjusted to account for the scaling factor of 0.81 arising from the application of phase-alternated Lee–Goldburg homonuclear decoupling [27,6].

field uniformity is successfully preserved for CP experiments and nearly matches the observe channel. Proper balancing of the RF circuit was essential for maintaining good ^{1}H B_1 field homogeneity in such an electrically long coil during cross-polarization experiments. If desired, B_1 uniformity at both frequencies can be further improved (at some expense to the ^{15}N channel efficiency) by varying the pitch of sample coil [30–32] with the wider gap between the 2nd and 3rd turns of the sample solenoid.

In a probe that is double-tuned by a trap inductor, the inductor value can be adjusted to produce the desired balance of high and low channel efficiency [33,11,22]. Analogously, it is helpful to adjust parameters of the $1/4\lambda$ coaxial line trap employed in this and other derivatives of the Cross–Hester–Waugh circuit according to experimental priorities. RF losses in the high frequency ^{1}H channel are minimized with the highest input impedance of the shorted coaxial line. This is achieved with lower dielectric constant, larger outer diameter of dielectric d_o and a coaxial diameter ratio d_o/d_i equal to 9.19, which corresponds to a characteristic line impedance of $Z_0 \sim 130\,\Omega$ in the air-dielectric line. The low-frequency ^{15}N channel, on the other hand, benefits from the largest inner conductor diameter d_i and from a higher dielectric constant that makes it shorter. By manipulating these parameters, one can tilt probe efficiency towards the ^{15}N or ^{1}H channel as needed for a particular experiment. Here, the trap was adjusted to provide sufficient ^{1}H decoupling field in a large sample coil for 2D PISEMA spectroscopy limited by a 300 W ^{1}H amplifier. With a larger ^{1}H amplifier, a different trap would allow the same experiment with better ^{15}N sensitivity.

Additional RF loss in the ^{1}H channel results from samples with higher hydration levels and salt concentrations, displaying the significant presence of electric fields inside the sample coil. Reducing the number of turns in the solenoid could help decrease electric field magnitude, but at a significant cost to the ^{15}N channel efficiency. Faraday shields [34,35] placed on the inside of the sample coil to shield against electric fields produced by the RF solenoid represent one possible approach for minimizing the electric field effect within the framework of this design.

Acknowledgments

This work was supported by the National High Magnetic Field Laboratory supported by NSF Cooperative agreement (DMR 00884173) and the State of Florida. The spectroscopy was supported by NSF MCB-0235774 to T.A.C. (FSU). M.C. acknowledges support from the Research Corporation (CC6128) and Dreyfus Foundation (SU-02-061). The authors also wish to acknowledge Richard Desilets for fabrication of the parts used in the probe, Tim J. Wagner for help with sample preparation, Kiran K. Shetty for help with probe testing, and Saikat Saha for helpful comments on the analysis.

References

[1] R.R. Ketchem, B. Roux, T.A. Cross, High-resolution polypeptide structure in a lamellar phase lipid environment from solid state NMR derived orientational constraints, Structure 5 (1997) 1655–1669.
[2] A.A. Nevzorov, M.F. Mesleh, S.J. Opella, Structure determination of aligned samples of membrane proteins by NMR spectroscopy, Magn. Reson. Chem. 42 (2004) 162–171.
[3] P. Walian, T.A. Cross, B.K. Jap, Structural genomics of membrane proteins, Genome Biol. 5 (2004).
[4] S.J. Opella, F.M. Marassi, Structure determination of membrane proteins by NMR spectroscopy, Chem. Rev. 104 (2004) 3587–3606.
[5] J.K. Denny, J.F. Wang, T.A. Cross, J.R. Quine, PISEMA powder patterns and PISA wheels, J. Magn. Reson. 152 (2001) 217–226.
[6] C.H. Wu, A. Ramamoorthy, S.J. Opella, High-resolution heteronuclear dipolar solid-state NMR spectroscopy, J. Magn. Reson. A 109 (1994) 270–272.
[7] J. Wang, S. Kim, F. Kovacs, T.A. Cross, Structure of the transmembrane region of the M2 protein H^+ channel, Protein Sci. 10 (2001) 2241–2250.
[8] S.J. Opella, A. Nevzorov, M.F. Mesleh, F.M. Marassi, Structure determination of membrane proteins by NMR spectroscopy, Biochem. Cell Biol. 80 (2002) 597–604.
[9] V.R. Cross, R.K. Hester, J.S. Waugh, Single coil probe with transmission-line tuning for nuclear magnetic double-resonance, Rev. Sci. Instrum. 47 (1976) 1486–1488.
[10] S. Kan, M. Fan, J. Courtieu, A single-coil triple resonance probe for NMR experiments, Rev. Sci. Instrum. 51 (1980) 887–890.
[11] F.D. Doty, R.R. Inners, P.D. Ellis, A multinuclear double-tuned probe for applications with solids or liquids utilizing lumped tuning elements, J. Magn. Reson. 43 (1981) 399–416.
[12] Y.J. Jiang, R.J. Pugmire, D.M. Grant, An efficient double-tuned ^{13}C/^{1}H probe circuit for CP/MAS NMR and its importance in linewidths, J. Magn. Reson. 71 (1987) 485–494.
[13] E.K. Paulson, R.W. Martin, K.W. Zilm, Cross polarization, radio frequency field homogeneity, and circuit balancing in high field solid-state NMR probes, J. Magn. Reson. 171 (2004) 314–323.
[14] Protein Data Bank # *1NYJ*.
[15] D. Salom, B.R. Hill, J.D. Lear, W.F. DeGrado, pH-dependent tetramerization and amantadine binding of the transmembrane helix of M2 from the influenza A virus, Biochemistry 39 (2000) 14160–14170.
[16] K. Nishimura, S.G. Kim, L. Zhang, T.A. Cross, The closed state of a H^+ channel helical bundle combining precise orientational and distance restraints from solid state NMR, Biochemistry 41 (2002) 13170–13177.
[17] F.A. Kovacs, J.K. Denny, Z. Song, J.R. Quine, T.A. Cross, Helix tilt of the M2 transmembrane peptide from influenza A virus: An intrinsic property, J. Mol. Biol. 295 (2000) 117–125.
[18] U. Silphaduang, E.J. Noga, Antimicrobials—Peptide antibiotics in mast cells of fish, Nature 414 (2001) 268–269.
[19] F. Engelke, Electromagnetic wave compression and radio frequency homogeneity in NMR solenoidal coils: computational approach, Concepts Magn. Reson. 15 (2002) 129–155.
[20] R.W. Martin, E.K. Paulson, K.W. Zilm, Design of a triple resonance magic angle sample spinning probe for high field solid state nuclear magnetic resonance, Rev. Sci. Instrum. 74 (2003) 3045–3061.
[21] O. Stuhlman Jr., S. Githens Jr., The magnetic field of a solenoid oscillating at radio frequencies, Rev. Sci. Instrum. 3 (1932) 561–571.
[22] Q.W. Zhang, H.M. Zhang, K.V. Lakshmi, D.K. Lee, C.H. Bradley, R.J. Witterbort, J. Magn. Reson. 132 (1998) 167–171.
[23] A.S. Lipton, J.A. Sears, P.D. Ellis, A general strategy for the NMR observation of half-integer quadrupolar nuclei in dilute environments, J. Magn. Reson. 151 (2001) 48–59.
[24] Standards Handbook for Wrought Copper and Copper Alloy Mill Products, Copper Development Association, Inc., Greenwich, CT (1985).

[25] S. Ramo, J.R. Whinnery, T. Van Duzer, Fields and Waves in Communication Electronics, third ed., Wiley, New York, 1994.
[26] C. Li, Y. Mo, J. Hu, E.Y. Chekmenev, C. Tian, F.P. Gao, R. Fu, P.L. Gor'kov, W.W. Brey, T.A. Cross, Analysis of RF heating and sample stability in aligned static solid state NMR spectroscopy, J. Magn. Reson. 179 (2006) 361–367.
[27] Z.T. Gu, S.J. Opella, Three-dimensional ^{13}C shift/^{1}H-^{15}N Coupling/^{15}N shift solid-state NMR correlation spectroscopy, J. Magn. Reson. 138 (1999) 193–198.
[28] C. Tian, P.F. Gao, L.H. Pinto, R.A. Lamb, T.A. Cross, Initial structural and dynamic characterization of the M2 protein transmembrane and amphipatic helices in lipid bilayers, Protein Sci. 12 (2003) 2597–2605.
[29] E.Y. Chekmenev, J. Hu, P.L. Gor'kov, W.W. Brey, T.A. Cross, A. Ruuge, A.I. Smirnov, ^{15}N and ^{31}P solid-state NMR study of transmembrane domain alignment of M2 protein of influenza A virus in hydrated cylindrical lipid bilayers confined to anodic aluminum oxide nanopores, J. Magn. Reson. 173 (2005) 322–327.
[30] S. Idziak, U. Haeberlen, Design and construction of a high homogeneity RF coil for solid-state multiple-pulse NMR, J. Magn. Reson. 50 (1982) 281.
[31] M.C. Leifer, RF solenoid with extended equiripple field profile, J. Magn. Reson. 105 (1993) 1.
[32] A.F. Privalov, S.V. Dvinskikh, H.-M. Vieth, Coil design for large volume high-B_1 homogeneity for solid-state NMR applications, J. Magn. Reson. 123 (1996) 157–160.
[33] D.I. Hoult, The NMR receiver: a description and analysis of design, Progr. In NMR Spect. 12 (1978) 41–77.
[34] D.G. Gadian, F.N.H. Robinson, Radiofrequency losses in NMR experiments on electrically conducting samples, J. Magn. Reson. 34 (1979) 449–455.
[35] D.W. Alderman, D.M. Grant, An efficient decoupler coil design which reduces heating in conductive samples in superconducting spectrometers, J. Magn. Reson. 36 (1979) 447–451.